

Improved CUT&RUN chromatin profiling tools

Michael P. Meers¹, Terri Bryson^{1,2} Jorja G. Henikoff¹ & Steven Henikoff^{1,2*}

¹Basic Sciences Division, Fred Hutchinson Cancer Research Center, 1100 N. Fairview Ave, Seattle, WA, 98109

²Howard Hughes Medical Institute, USA

*Corresponding author

Abstract

Previously we described a novel alternative to Chromatin Immunoprecipitation, CUT&RUN, in which unfixed permeabilized cells are incubated with antibody, followed by binding of a Protein A-Micrococcal Nuclease (pA/MNase) fusion protein (Skene and Henikoff, 2017). Here we introduce three enhancements to CUT&RUN: A hybrid Protein A-Protein G-MNase construct that expands antibody compatibility and simplifies purification, a modified digestion protocol that inhibits premature release of the nuclease-bound complex, and a calibration strategy based on carry-over of *E. coli* DNA introduced with the fusion protein. These new features, coupled with the previously described low-cost, high efficiency, high reproducibility and high-throughput capability of CUT&RUN make it the method of choice for routine epigenomic profiling.

Introduction

Profiling the chromatin landscape for specific components is one of the most widely used methods in biology, and over the past decade, chromatin immunoprecipitation (ChIP) followed by sequencing (ChIP-seq) has become practically synonymous with genome-wide chromatin profiling (Landt et al., 2012; Schubert, 2018). However, the most widely used ChIP-seq protocols have limitations and are subject to artifacts (Jain et al., 2015; Park et al., 2013; Teves et al., 2016; Teytelman et al., 2013), of which only some have been addressed by methodological improvements (Brind'Amour et al., 2015; Kasinathan et al., 2014; Rhee and Pugh, 2011; Rossi et al., 2018; van Galen et al., 2016). An inherent limitation to ChIP is that solubilization of chromatin, whether by sonication or enzymatic digestion, results in sampling from the entire solubilized genome, and this requires very deep sequencing so that the sites of targeted protein binding can be resolved above background (Landt et al., 2012). To overcome this limitation, we introduced Cleavage Under Targets and Release Using Nuclease (CUT&RUN) (Skene and Henikoff, 2017), which is based on the chromatin immunocleavage (ChIC) targeted nuclease strategy (Schmid et al., 2004): Successive incubation of unfixed cells or nuclei with an antibody and a Protein A-Micrococcal Nuclease (pA/MNase) fusion protein is followed by activation of MNase with calcium. In CUT&RUN, cells or nuclei remain intact throughout the procedure and only the targeted sites of binding are released into solution. Our CUT&RUN method dramatically reduced non-specific backgrounds, such that ~10-fold lower sequencing depth was required to obtain similar peak-calling performance (Skene and Henikoff, 2017). In addition, CUT&RUN provides near base-pair resolution, and our most recently published benchtop protocol is capable of profiling ~100 human cells for an abundant histone modification and ~1000 cells for a transcription factor (Skene et al., 2018). The simplicity of CUT&RUN has also resulted in a fully automated robotic version (AutoCUT&RUN) in which the high reproducibility and low cost makes it ideally suited for high-throughput epigenomic profiling of clinical samples (Janssens et al., 2018). Other advances based on our original CUT&RUN publication include CUT&RUN.Salt for fractionation of chromatin based on solubility (Thakur and Henikoff, 2018) and CUT&RUN.ChIP for profiling specific protein components within complexes released by CUT&RUN digestion (Brahma and Henikoff, 2019). CUT&RUN has

also been adopted by others (Ahmad and Spens, 2018; Daneshvar et al., 2019; de Bock et al., 2018; Ernst et al., 2019; Federation et al., 2018; Hainer et al., 2019; Hainer and Fazio, 2019; Hyle et al., 2019; Inoue et al., 2018; Liu et al., 2018; Menon et al., 2019; Oomen et al., 2019; Park et al., 2019; Roth et al., 2018; Uyehara and McKay, 2019; Zhang et al., 2019; Zheng and Gehring, 2019), and since publication of our *eLife* paper we have distributed materials to >600 laboratories world-wide, with user questions and answers fielded interactively on our open-access Protocols.io site (dx.doi.org/10.17504/protocols.io.zcpf2vn).

Broad implementation of CUT&RUN requires reagent standardization, and the rapid adoption of CUT&RUN by the larger community of researchers motivates the enhancements described here. First, the method requires a fusion protein that is not at this writing commercially available, and the published pA/MNase purification protocol is cumbersome, which effectively restricts dissemination of the method. Therefore we have produced an improved construct with a 6-His-Tag that can be easily purified using a commercial kit, and by using a Protein A-Protein G hybrid, the fusion protein binds avidly to mouse antibodies, which bind only weakly to Protein A. Second, the original protocols are sensitive to digestion time, in that under-digestion results in low yield and over-digestion can result in pre-mature release of pA/MNase-bound complexes that can digest accessible DNA sites. To address this limitation, we have modified the protocol such that premature release is reduced, allowing digestion to near-completion for high yields with less background. Third, the current CUT&RUN protocol recommends a spike-in of heterologous DNA at the release step to compare samples in a series. Here we demonstrate that adding a spike-in is unnecessary, because the carry-over of *E. coli* DNA from purification of pA/MNase or pAG/MNase is sufficient to calibrate samples in a series.

Results and Discussion

An improved CUT&RUN vector

The pA/MNase fusion protein produced by the pK19-pA-MN plasmid (Schmid et al., 2004) requires purification from lysates of *Escherichia coli* overexpressing cells using an immunoglobulin G (IgG) column, and elution with low pH followed by neutralization has

81 resulted in variations between batches. To improve the purification protocol, we added a 6-His
82 tag (Bornhorst and Falke, 2000) into the pK19-pA-MN fusion protein (Figure 1A and Figure 1 –
83 figure supplement 1A). This allowed for simple and gentle purification on a nickel resin column
84 (Figure 1 – figure supplement 1B). In addition, we found that a commercial 6-His-cobalt resin kit
85 also yielded pure highly active enzyme from a 20 ml culture, enough for ~10,000 reactions.
86 Even when used in excess, there is no increase in release of background fragments (Figure 1 –
87 figure supplement 2), which indicates that the washes are effective in removing unbound fusion
88 protein.

89
90 In principle an epitope-tagged pAG/MNase could be used for chromatin pull-down from a
91 CUT&RUN supernatant in sequential strategies like CUT&RUN.ChIP (17). However, in practice
92 use of the 6-His tag is complicated by the requirement for a chelating agent to release the
93 protein from the nickel resin. Therefore, we also added an HA (hemagglutinin) tag, which could
94 be used to affinity-purify the complex of a directly bound chromatin particle with a primary
95 antibody and the fusion protein.

96
97 Protein A binds well to rabbit, goat, donkey and guinea pig IgG antibodies, but poorly to mouse
98 IgG1, and so for most mouse antibodies, Protein G is generally used (Fishman and Berg, 2019).
99 To further improve the versatility of the MNase fusion protein, we encoded a single Protein G
100 domain adjacent to the Protein A domain in the pK19-pA-MN plasmid (Eliasson et al., 1988). In
101 addition, we mutated three residues in the Protein G coding sequence to further increase
102 binding for rabbit antibodies (Jha et al., 2014). This resulted in a fusion protein that binds
103 strongly to most commercial antibodies without requiring a secondary antibody. We found that
104 for ordinary CUT&RUN applications pAG/MNase behaves very similarly to pA/MNase, but is
105 more easily purified and is more versatile, for example allowing us to perform CUT&RUN
106 without requiring a secondary antibody for mouse primary monoclonal antibodies (Figure 1B).

107 108 **Preventing premature release during CUT&RUN digestion**

When fragments are released by cleavage in the presence of Ca^{++} ions, the associated pA/MNase complex can digest accessible DNA (Skene and Henikoff, 2017). Although performing digestion at 0°C minimizes this artifact, eliminating premature release during digestion would allow for more complete release of target-specific fragments. Based on the observation that nucleosome core particles aggregate in high-divalent-cation and low-salt conditions (de Frutos et al., 2001), we wondered whether these conditions would prevent premature release of chromatin particles *in situ*. Therefore, we performed digestions in 10 mM CaCl_2 and 3.5 mM HEPES pH 7.5. Under these high-calcium/low-salt conditions, chromatin is digested with no detectable release of fragments into the supernatant (Figure 2). Reactions are halted by transferring the tube to a magnet, removing the liquid, and adding elution buffer containing 150 mM NaCl, 20 mM EGTA and 25 $\mu\text{g}/\text{ml}$ RNase A, which releases the small DNA fragments into the supernatant. These conditions are compatible with direct end-polishing and ligation used for AutoCUT&RUN (Janssens et al., 2018). Furthermore, retention of the cleaved fragments within the nucleus under high-divalent cation/low-salt conditions could facilitate single-cell application of CUT&RUN.

The high-calcium/low-salt protocol provided similar results using either pA/MNase and pAG/MNase (Figure 3). We also obtained similar results with either protocol for digestion time points over a ~ 30 -fold range and for both supernatant and total DNA extraction (Figure 4 – figure supplement 1). For antibodies to H3K27ac, libraries produced using the high-calcium/low-salt protocol showed improved consistency relative to the standard protocol when digested over an extended time-course (Figure 4), presumably because preventing release of particles during digestion avoids their premature release where they would artifactually digest accessible DNA. The close correlations between high-calcium/low-salt H3K27ac datasets for time points over a ~ 100 -fold range occur with corresponding increases in the yield of fragments released into the supernatant during subsequent elution (Figure 4 – figure supplement 2). This indicates that longer digestion times result in higher yields, with high signal-to-noise throughout the digestion series (Figure 4). Thus, this modification of CUT&RUN can reduce the

137 risk of overdigestion for abundant epitopes such as H3K27ac, where premature release of pA-
138 MNase-bound chromatin particles can increase background.

139
140 We previously showed that CUT&RUN can be performed on insoluble protein complexes by
141 extracting total DNA (Skene and Henikoff, 2017) or by performing salt fractionation of the bead-
142 bound cells and extracting DNA from the residual pellet (Thakur and Henikoff, 2018). In either
143 case, large DNA fragments were depleted using SPRI (AMPure XP) beads before library
144 preparation. RNA polymerase II (RNAPII) from animal cells is insoluble when engaged (Mayer et
145 al., 2015; Weber et al., 2014), and requires harsh treatments for quantitative profiling using
146 ChIP (Skene and Henikoff, 2015). To determine whether CUT&RUN can be used for insoluble
147 chromatin complexes, we profiled Serine-5-phosphate on the C-terminal domain (CTD) of the
148 Rpb1 subunit of RNAPII using both extraction of supernatant and of total DNA. This CTD
149 phosphorylation is enriched in the initiating form of RNAPII, and we observed similar genic
150 profiles for supernatant and total DNA (Figure 1B).

151 152 **Calibration using *E. coli* carry-over DNA**

153 Comparing samples in a series typically requires calibration for experimental quality and
154 sequencing read depth. It is common to use background levels to calibrate ChIP-seq samples in
155 a series and to define and compare peaks for peak-calling (Landt et al., 2012). However, the
156 extremely low backgrounds of CUT&RUN led us to a calibration strategy based on spike-in of
157 heterologous DNA, which has been generally recommended for all situations in which samples
158 in a series are to be compared (Chen et al., 2015; Hu et al., 2015). In our current spike-in
159 protocol, the heterologous DNA, which is typically DNA purified from an MNase digest of yeast
160 *Saccharomyces cerevisiae* or *Drosophila melanogaster* chromatin, is added when stopping a
161 reaction, and we adopted this spike-in procedure for the high-calcium/low-salt protocol
162 described in the previous section. Interestingly, we noticed that mapping reads to both the
163 spike-in genome and the *E. coli* genome resulted in almost perfect correlation ($R^2=0.97$)
164 between *S. cerevisiae* and *E. coli* in an experiment using pA/MNase in which the number of cells
165 was varied over several orders of magnitude (Figure 5A). Near-perfect correlations ($R^2=0.96$ -

0.99) between yeast spike-in and carry-over *E. coli* DNA were also seen in series using the same batch of pAG/MNase with high-calcium/low-salt digestion conditions (Figure 5B), and for both supernatant release and extraction and total DNA extraction (Figure 5C-D). These strong positive correlations are not accounted for by cross-mapping of the yeast spike-in to the *E. coli* genome, because omitting the spike-in for a low-abundance epitope resulted in very few yeast counts with high levels of *E. coli* counts (blue symbol in Figure 5C-D panels). As the source of *E. coli* DNA is carried over from purification of pA/MNase and pAG/MNase, the close correspondence provides confirmation of the accuracy of our heterologous spike-in procedure (Skene and Henikoff, 2017). Moreover, as carry-over *E. coli* DNA is introduced at an earlier step, and is cleaved to small mappable fragments that are released during digestion and elution, it provides a more desirable calibration standard than using heterologous DNA (Chen et al., 2015; Hu et al., 2015). High correlations were also seen between *S. cerevisiae* spike-in and *E. coli* carry-over DNA for pA-MNase in batches that we have distributed (Table 1). Therefore, data for nearly all CUT&RUN experiments performed thus far can be recalibrated *post-hoc* whether or not a spike-in calibration standard had been added.

To explain the presence of carry-over *E. coli* DNA in proportion to the amount of yeast spike-in DNA, which is constant between samples in a series, we can exclude intracellular binding, because we observe proportionality between *E. coli* and yeast reads despite varying human cell numbers over two orders of magnitude (Figure 5A). Rather, we note that Concanavalin A binds to glycosylated immunoglobulins, and so the successive treatments of Con A bead-bound cells with excess antibody and Protein A(G)/MNase fusion protein will affix an amount of carry-over *E. coli* DNA to beads in proportion to the number of beads. Our use of a constant number of beads for all samples in a series to be compared would then have resulted in a constant amount of carry-over *E. coli* DNA. A similar inference of *E. coli* carry-over DNA suitable for calibration was noted for CUT&Tag (Kaya-Okur et al., 2019), which suggests successive binding of antibodies and Protein A-Tn5 to the Con A beads used to immobilize cells. Thus our calibration strategy might serve as a more general replacement for conventional spike-ins.

Conclusions

Since its introduction in our original *eLife* paper (Skene and Henikoff, 2017), the advantages of CUT&RUN over ChIP-seq has led to its rapid adoption, including publication of new CUT&RUN protocols for low cell numbers (Hainer and Fazio, 2019; Skene et al., 2018), for plant tissues (Zheng and Gehring, 2019) and for high-throughput (Janssens et al., 2018). The new CUT&RUN advances that we describe here are likely to be useful when applied in all of these protocols. Our improved CUT&RUN fusion construct simplifies reagent purification and eliminates the requirement for a secondary antibody against mouse primary antibodies. Our high-calcium/low-salt protocol minimizes time-dependent variability. Our discovery that carry-over *E. coli* DNA almost perfectly correlates with an added spike-in upgrades a contaminant to a resource that can be used as a spike-in calibration proxy, even *post-hoc* simply by counting reads mapping to the *E. coli* genome in existing CUT&RUN datasets.

Materials and methods

Key Resources Table

Reagent type (species) or resource	Designation	Source or reference	Identifiers	Additional information
cell line (Human)	K562	ATCC	#CCL-243	RRID: CVCL_0004
cell line (Human)	H1 embryonic stem cells	WiCell	#WA01-lot#WB35186	RRID: CVCL_9771
cell line (Human)	DE definitive endoderm	WiCell	#WA01-lot#WB35186	Differentiated from H1 embryonic stem cells
biological sample (Escherichia coli)	JM101 cells	Agilent	#200234	
antibody	rabbit polyclonal anti-NPAT	Thermo	PA5-66839	Concentration: 1:100; RRID:AB_2663287
antibody	guinea pig polyclonal anti-rabbit IgG	Antibodies Online	ABIN101961	Concentration: 1:100; RRID: AB_10775589
antibody	rabbit polyclonal anti-mouse IgG	Abcam	46540	Concentration: 1:100; RRID: AB_2614925
antibody	rabbit monoclonal anti-RNAPII-Ser5	Cell Signaling	D9N51	Concentration:

				1:100
antibody	mouse monoclonal anti-RNAPII-Ser5	Abcam	5408	Concentration: 1:100; RRID:AB_304868
antibody	rabbit monoclonal anti-H3K27me3	Cell Signaling	9733	Concentration: 1:100; RRID: AB_2616029
antibody	rabbit polyclonal anti-H3K4me2	Upstate	07-730	Concentration: 1:100; RRID: AB_11213050
antibody	rabbit monoclonal anti-H3K27ac	Millipore	MABE647	Concentration: 1:100;
antibody	rabbit polyclonal anti-H3K27ac	Abcam	4729	Concentration: 1:100; RRID: AB_2118291
antibody	rabbit polyclonal anti-CTCF	Millipore	07-729	Concentration: 1:100; RRID: AB_441965
antibody	rabbit monoclonal anti-Sox2	Abcam	ab92494	Concentration: 1:50; RRID: AB_10585428
antibody	rabbit polyclonal anti-FoxA2	Millipore	07-633	Concentration: 1:50; RRID: AB_390153
recombinant DNA reagent	AG-ERH-MNase-6xHIS-HA (plasmid)		Progenitors: pK19-pA-MN; gBlocks	
recombinant DNA reagent	pK19-pA-MN	PMID: 15469830		Gift from author
sequence-based reagent	gBlock Hemagglutinin and 6-histidine tags ;gattacaGAAGACAACGCTGATTACAG GTCAAGGCGGtGGTGGcTCTGGgGGc GGgGGcTCGGGtGGtGGgGGcTCAcac catcaccatcaccatGGCGGtGGTGGcTC TTACCCATACGATGTTCCAGATTACG CTtaatgaGGATCCgattaca	Integrated DNA Technologies (IDT)		
sequence-based reagent	gBLOCK PrtG_ERH Codon optimized; AGCAGAAGCTAAAAAGCTAAACGAT GCTCAAGCACCAAAAAACAATTATAA ATTAGTCATCAACGGGAAAACGCTG AAGGGTGAAACCACGACAGAGGCCG TAGATGCGGAGACAGCGGAGCGCCA CTTTAAGCAATACGCGAATGATAACG GTGTAGACGGCGAGTGGACCTACGA CGACGCGACAAAGACCTTTACCGTCA CGGAGAAACCTGAGGTTATCGACGC GTCTGAGTTGACGCCAGCCGTAGAT GACGATAAAGAATTCGCAACTTCAAC TAAAAAATTAC	Integrated DNA Technologies (IDT)		

peptide, recombinant protein	pA/MNase	PMID: 15469830		purified as described in PMID: 15469830 and supplementary
peptide, recombinant protein	pAG/MNase	This paper		Purified from modified plasmid pAG-ERH-MNase-6xHIS-HA in S. Henikoff Lab
commercial assay or kit	Pull-Down PolyHis Protein:Protein Interaction Kit	Thermo	#21277	
commercial assay or kit	StemDiff Definitive Endoderm Kit	StemCell Technologies	#05110	
other	Concanavalin A coated magnetic beads	Bangs Laboratories	#BP-531	
other	Gibson Assembly	New England Biolabs	#E2611	
other	Chicken egg white lysozyme	EMD Millipore	#71412	
other	Zwittergent 3-10 detergent (0.03%)	EMD Millipore	#693021	
Chemical compound, drug	Digitonin	EMD Millipore	#300410	
Chemical compound, drug	Roche Complete Protease Inhibitor EDTA-free tablets	Sigma Aldrich	5056489001	
Chemical compound, drug	RNase A Dnase- and protease-free	Thermo	ENO531	10 mg/ml
Chemical compound, drug	Proteinase K	Thermo	EO0492	
Chemical compound, drug	Glycogen	Sigma-Aldrich	10930193001	
Chemical compound, drug	Spermidine	Sigma-Aldrich	#S0266	

Cell culture

K562 cells were purchased from ATCC (#CCL-243) and H1 hESCs were purchased from WiCell (WiCell#WA01-lot#WB35186) and cultured as previously described (15). Definitive endoderm (DE) was derived from a culture of H1 hESCs using the StemDiff Definitive Endoderm kit (StemCell Technologies). All tested negative for mycoplasma contamination using MycoProbe kit.

Construction and purification of an improved IgG-affinity/MNase fusion protein

Hemagglutinin and 6-histidine tags were added to the carboxyl-terminus of pA-MNase (Schmid et al., 2004) using a commercially synthesized dsDNA fragment (gBlock®) from Integrated DNA Technologies (IDT), which contains the coding sequence for both tags, glycine-rich flexible linkers and includes restriction sites for cloning. Another IDT gBlock® containing the optimized protein-G coding sequence and homologous flanking regions to the site of insertion, was introduced via PCR overlap extension using Gibson Assembly® Master Mix (New England Biolabs cat. #E2611), following the manufacturer's instructions. The sequence-verified construct was transformed into JM101 cells (Agilent Technologies cat. #200234) for expression, cultured in NZCYM-Kanamycin (50 µg/ml) and induced with 2 mM Isopropyl β-D-1-thiogalactopyranoside following standard protein expression and purification protocols. The cell pellet was resuspended in 10 ml Lysis Buffer, consisting of 10mM Tris-HCL pH 7.5, 300mM NaCl, 10mM Imidazole, 5mM beta-mercaptoethanol, and EDTA-free protease inhibitor tablets at the recommended concentration (Sigma-Aldrich cat. #5056489001). Lysis using chicken egg white lysozyme (10 mg/mL solution, EMD cat. #71412 solution) was followed by sonication with a Branson Sonifier blunt-end adapter at output level 4, 45 seconds intervals for 5-10 rounds or until turbidity was reduced. The lysate was cleared by high-speed centrifugation and purified over a nickel-agarose column, taking advantage of the poly-histidine tag for efficient purification via immobilized metal affinity chromatography. Cleared lysate was applied to a 20 ml disposable gravity-flow column 1.5 ml (0.75 ml bed volume) of NI-NTA agarose (Qiagen cat. #30210), washed twice in three bed volumes of Lysis Buffer. Lysate was applied followed by two washes at five bed volumes of 10 mM Tris-HCl pH 7.5, 300 mM NaCl, 20 mM Imidazole, 0.03% ZWITTERGENT 3-10 Detergent (EMD Millipore cat. #693021) and EDTA-free protease inhibitor tablets. Elution was performed with 1 ml 10 mM Tris-HCl pH 7.5, 300 mM NaCl, 250 mM Imidazole and EDTA-free protease inhibitor tablets. Eluate was dialyzed twice against a 750 ml volume of 10mM Tris-HCl pH 7.5 , 150 mM NaCl, 1 mM EDTA, 1 mM PMSF to remove imidazole. Glycerol was then added to 50%, aliquots stored at –80 °C for long term storage and –20 °C for working stocks.

For purification, we used either the nickel-based protocol or the Pierce Cobalt kit (Pull-Down PolyHis Protein:Protein Interaction Kit cat. #21277 from Thermo Fisher). Similar results were obtained using either the nickel or cobalt protocol, although the cobalt kit alleviated the need for a sonicator, using a fifth of the starting material from either fresh culture or a cell pellet frozen in lysis buffer, and yielded more protein per volume of starting material. With the cobalt kit, 20 ml of culture yielded ~100 µg of fusion protein.

CUT&RUN using high-calcium/low-salt digestion conditions

Log-phase cultures of K562 cells were harvested, washed, and bound to activated Concanavalin A-coated magnetic beads, then permeabilized with Wash buffer (20 mM HEPES, pH7.5, 150 mM NaCl, 0.5 mM spermidine and a Roche complete tablet per 50 ml) containing 0.05% Digitonin (Dig-Wash) as described (Skene et al., 2018). The bead-cell slurry was incubated with antibody in a 50-100 µL volume for 2 hr at room temperature or at 4°C overnight on a nutator or rotator essentially as described (Skene et al., 2018). In some experiments, cells were permeabilized and antibody was added and incubated 2 hr to 3 days prior to addition of ConA beads with gentle vortexing; similar results were obtained (*e.g.* Figure 2B-D), although with lower yields. After 2-3 washes in 1 ml Dig-wash, beads were resuspended in 50-100 µL pA/MNase or pAG/MNase and incubated for 1 hr at room temperature. After 2 washes in Dig-wash, beads were resuspended in low-salt rinse buffer (20 mM HEPES, pH7.5, 0.5 mM spermidine, a Roche mini-complete tablet per 10 ml and 0.05% Digitonin). Tubes were chilled to 0°C, the liquid was removed on a magnet stand, and ice-cold calcium incubation buffer (3.5 mM HEPES pH 7.5, 10 mM CaCl₂, 0.05% Digitonin) was added while gently vortexing. Tubes were replaced on ice during the incubation for times indicated in each experiment, and within 30 seconds of the end of the incubation period the tubes were replaced on the magnet, and upon clearing, the liquid was removed, followed by immediate addition of EGTA-STOP buffer (170 mM NaCl, 20 mM EGTA, 0.05% Digitonin, 20 µg/ml glycogen, 25 µg/ml RNase A, 2 pg/ml *S. cerevisiae* fragmented nucleosomal DNA). Beads were incubated at 37°C for 30 min, replaced on a magnet stand and the liquid was removed to a fresh tube and DNA was extracted as described (Skene et al., 2018). A detailed step-by-step protocol is available at <https://www.protocols.io/view/cut-amp-run->

targeted-in-situ-genome-wide-profiling-zcpf2vn. Extraction of pellet and total DNA was performed essentially as described (Skene and Henikoff, 2017; Thakur and Henikoff, 2018).

DNA sequencing and data processing. The size distribution of libraries was determined by Agilent 4200 TapeStation analysis, and libraries were mixed to achieve equal representation as desired aiming for a final concentration as recommended by the manufacturer. Paired-end Illumina sequencing was performed on the barcoded libraries following the manufacturer's instructions. Paired-end reads were aligned using Bowtie2 version 2.2.5 with options: --local --very-sensitive-local --no-unal --no-mixed --no-discordant --phred33 -I 10 -X 700. For MACS2 peak calling, parameters used were macs2 callpeak -t input_file -p 1e-5 -f BEDPE/BED(Paired End vs. Single End sequencing data) --keep-dup all -n out_name. Some datasets showed contamination by sequences of undetermined origin consisting of the sequence (TA)_n. To avoid cross-mapping, we searched blastn for TATATATATATATATATATATATAT against hg19, collapsed the overlapping hits into 34,832 regions and intersected with sequencing datasets, keeping only the fragments that did not overlap any of these regions.

Evaluating time-course data

If digestion and fragment release into the supernatant occur linearly with time of digestion until all fragments within a population are released, then we expect that CUT&RUN features will be linearly correlated within a time-course series. For CTCF, features were significant CTCF motifs intersecting with DNaseI hypersensitive sites (Skene and Henikoff, 2017). For H3K27Ac and H3K4me2, we called peaks using MACS2 and calculated the Pearson correlation coefficients between time points, displayed as a matrix of R^2 values, using the following procedure:

1) Aligned fastq files to unmasked genomic sequence using Bowtie2 version 2.2.5 to UCSC hg19 with parameters: `--end-to-end --very-sensitive --no-mixed --no-discordant -q --phred33 -I 10 -X 700`.

2) Extracted properly paired read fragments from the alignments and pooled fragments from multiple samples.

3) Compared pooled fragments with (TA)_n regions of hg19 and kept those fragments that did NOT overlap any (TA)_n region using bedtools 2.21.0 with parameters: intersect -v -a fragments.bed -b TATA_regions.bed > fragments_not_TATA.bed.

4) Found peaks using macs2 2.1.1.20160309 with parameters: callpeak -t fragments_not_mask.bed -f BED -g hs --keep-dup all -p 1e-5 -n not_mask --SPMR.

5) Made scaled fractional count bedgraph files for each sample from bed files made in step 2. The value at each base pair is the fraction of counts times the size of hg19 so if the counts were uniformly distributed the value would be 1 at each bp.

6) Extracted bedgraph values for ±150 bps around peak summits for IgG sample and computed their means, which resulted in one mean score per peak.

7) Removed peaks from macs2 results in step 4 if the mean score was greater than the 99th percentile of all IgG scores to make a subset of the peaks lacking the most extreme outliers.

8) Extracted bedgraph values for ±150 bps around the subset of peak summits from step 7 for all samples and computed their means, which resulted in a matrix with columns corresponding to samples and one row per peak.

9) Computed correlations of matrix in 8 using R 3.2.2 cor(matrix, use="complete.obs") command.

Availability

The plasmid pAG-ERH-MNase-6xHIS-HA is available from Addgene. Sequencing datasets are available from GEO (GSE126612).

Acknowledgements

We thank Christine Codomo and Tayler Hentges for technical support. We also thank all members of the Henikoff lab for valuable discussions and Kami Ahmad, Brian Freie and Bob Eisenman for comments on the manuscript. This work was supported by the Howard Hughes Medical Institute, and a grant from the National Institutes of Health (4DN T CPA A093) and the Chan-Zuckerberg Initiative.

Competing interests

The authors declare no competing interests.

References

- Ahmad, K., and Spens, A. (2018). Separate Polycomb Response Elements control chromatin state and activation of the vestigial gene. *biorxiv* <https://www.biorxiv.org/content/early/2018/12/05/488478>.
- Bornhorst, J.A., and Falke, J.J. (2000). Purification of proteins using polyhistidine affinity tags. *Methods Enzymol* 326, 245-254.
- Brahma, S., and Henikoff, S. (2019). RSC-Associated Subnucleosomes Define MNase-Sensitive Promoters in Yeast. *Mol Cell* 73, 238-249.
- Brind'Amour, J., Liu, S., Hudson, M., Chen, C., Karimi, M.M., and Lorincz, M.C. (2015). An ultra-low-input native ChIP-seq protocol for genome-wide profiling of rare cell populations. *Nat Commun* 6, 6033.
- Chen, K., Hu, Z., Xia, Z., Zhao, D., Li, W., and Tyler, J.K. (2015). The Overlooked Fact: Fundamental Need for Spike-In Control for Virtually All Genome-Wide Analyses. *Mol Cell Biol* 36, 662-667.
- Daneshvar, K., Ardehal, M.V., Klein, I.A., Kratkiewicz, A.J., Zhou, C., Mahpour, A., Cook, B.M., Li, W., Pondick, J.V., Moran, S.P., *et al.* (2019). lncRNA DIGIT and BRD3 protein form phase-separated condensates to regulate endoderm differentiation. *biorxiv* <https://www.biorxiv.org/content/10.1101/547513v1>, 547513v547511.
- de Bock, C.E., Demeyer, S., Degryse, S., Verbeke, D., Sweron, B., Gielen, O., Vandepoel, R., Vicente, C., Vanden Bempt, M., Dagklis, A., *et al.* (2018). HOXA9 Cooperates with Activated JAK/STAT Signaling to Drive Leukemia Development. *Cancer discovery* 8, 616-631.
- de Frutos, M., Raspaud, E., Leforestier, A., and Livolant, F. (2001). Aggregation of nucleosomes by divalent cations. *Biophys J* 81, 1127-1132.
- Eliasson, M., Olsson, A., Palmcrantz, E., Wiberg, K., Inganas, M., Guss, B., Lindberg, M., and Uhlen, M. (1988). Chimeric IgG-binding receptors engineered from staphylococcal protein A and streptococcal protein G. *J Biol Chem* 263, 4323-4327.
- Ernst, C., Eling, N., Martinez-Jimenez, C.P., Marioni, J.C., and Odom, D.T. (2019). Staged developmental mapping and X chromosome transcriptional dynamics during mouse spermatogenesis. *Nat Commun* 10, 1251.

367 Federation, A.J., Nandakumar, V., Wang, H., Searle, B., Pino, L., Merrihew, G., Ting, S., Howard,
 368 N., Kutayavin, T., MacCoss, M.J., *et al.* (2018). Quantification of nuclear protein dynamics reveals
 369 chromatin remodeling during acute protein degradation. *bioRxiv*
 370 <https://www.biorxiv.org/content/early/2018/06/30/345686>.

371 Fishman, J.B., and Berg, E.A. (2019). Protein A and Protein G Purification of Antibodies. *Cold*
 372 *Spring Harbor protocols 2019*, pdb prot099143.

373 Hainer, S.J., Boškovic, A., McCannell, K.N., Rando, O.J., and Fazio, T.G. (2019). Profiling of
 374 pluripotency factors in individual stem cells and early embryos. *Cell* *doi:*
 375 *10.1016/j.cell.2019.03.014*.

376 Hainer, S.J., and Fazio, T.G. (2019). High-Resolution Chromatin Profiling Using CUT&RUN.
 377 *Current protocols in molecular biology* / edited by Frederick M Ausubel [et al], e85.

378 Hu, B., Petela, N., Kurze, A., Chan, K.L., Chapard, C., and Nasmyth, K. (2015). Biological
 379 chromodynamics: a general method for measuring protein occupancy across the genome by
 380 calibrating ChIP-seq. *Nucleic Acids Res* *43*, e132.

381 Hyle, J., Zhang, Y., Wright, S., Xu, B., Shao, Y., Easton, J., Tian, L., Feng, R., Xu, P., and Li, C.
 382 (2019). Acute depletion of CTCF directly affects MYC regulation through loss of enhancer-
 383 promoter looping. *Nucleic Acids Res*.

384 Inoue, A., Chen, Z., Yin, Q., and Zhang, Y. (2018). Maternal Eed knockout causes loss of
 385 H3K27me3 imprinting and random X inactivation in the extraembryonic cells. *Genes Dev* *32*,
 386 1525-1536.

387 Jain, D., Baldi, S., Zabel, A., Straub, T., and Becker, P.B. (2015). Active promoters give rise to
 388 false positive 'Phantom Peaks' in ChIP-seq experiments. *Nucleic Acids Res* *43*, 6959-6968.

389 Janssens, D.H., Wu, S.J., Sarthy, J.F., Meers, M.P., Myers, C.H., Olson, J.M., Ahmad, K., and
 390 Henikoff, S. (2018). Automated in situ chromatin profiling efficiently resolves cell types and
 391 gene regulatory programs. *Epigenetics Chromatin* *11*, 74.

392 Jha, R.K., Gaiotto, T., Bradbury, A.R., and Strauss, C.E. (2014). An improved Protein G with
 393 higher affinity for human/rabbit IgG Fc domains exploiting a computationally designed polar
 394 network. *Protein engineering, design & selection : PEDS* *27*, 127-134.

395 Kasinathan, S., Orsi, G.A., Zentner, G.E., Ahmad, K., and Henikoff, S. (2014). High-resolution
 396 mapping of transcription factor binding sites on native chromatin. *Nature Methods* *11*, 203-209.

397 Kaya-Okur, H.S., Wu, S.J., Codomo, C.A., Pledger, E.S., Bryson, T.D., Henikoff, J.G., Ahmad, K.,
 398 and Henikoff, S. (2019). CUT&Tag for efficient epigenomic profiling of small samples and single
 399 cells. *Nat Commun* *10*, 1930.

400 Landt, S.G., Marinov, G.K., Kundaje, A., Kheradpour, P., Pauli, F., Batzoglou, S., Bernstein, B.E.,
 401 Bickel, P., Brown, J.B., Cayting, P., *et al.* (2012). ChIP-seq guidelines and practices of the
 402 ENCODE and modENCODE consortia. *Genome Res* 22, 1813-1831.

403 Liu, N., Hargreaves, V.V., Zhu, Q., Kurland, J.V., Hong, J., Kim, W., Sher, F., Macias-Trevino, C.,
 404 Rogers, J.M., Kurita, R., *et al.* (2018). Direct Promoter Repression by BCL11A Controls the Fetal
 405 to Adult Hemoglobin Switch. *Cell* 173, 430-442.

406 Mayer, A., Iulio, J., Maleri, S., Eser, U., Vierstra, J., Reynolds, A., Sandstrom, R.,
 407 Stamatoyannopoulos, J.A., and Churchman, S. (2015). Native elongating transcript sequencing
 408 reveals human transcriptional activity at nucleotide resolution. *Cell* 161, 541-554.

409 Menon, D.U., Shibata, Y., Mu, W., and Magnuson, T. (2019). Mammalian SWI/SNF collaborates
 410 with a polycomb-associated protein to regulate male germ line transcription in the mouse.
 411 *Development*.

412 Oomen, M.E., Hansen, A.S., Liu, Y., Darzacq, X., and Dekker, J. (2019). CTCF sites display cell
 413 cycle-dependent dynamics in factor binding and nucleosome positioning. *Genome Res* 29, 236-
 414 249.

415 Park, D., Lee, Y., Bhupindersingh, G., and Iyer, V.R. (2013). Widespread misinterpretable ChIP-
 416 seq bias in yeast. *PLoS One* 8, e83506.

417 Park, S.M., Cho, H., Thornton, A.M., Barlowe, T.S., Chou, T., Chhangawala, S., Fairchild, L.,
 418 Taggart, J., Chow, A., Schurer, A., *et al.* (2019). IKZF2 Drives Leukemia Stem Cell Self-Renewal
 419 and Inhibits Myeloid Differentiation. *Cell Stem Cell* 24, 153-165.

420 Rhee, H.S., and Pugh, B.F. (2011). Comprehensive genome-wide protein-DNA interactions
 421 detected at single-nucleotide resolution. *Cell* 147, 1408-1419.

422 Rossi, M.J., Lai, W.K.M., and Pugh, B.F. (2018). Simplified ChIP-exo assays. *Nat Commun* 9, 2842.

423 Roth, T.L., Puig-Saus, C., Yu, R., Shifrut, E., Carnevale, J., Li, P.J., Hiatt, J., Saco, J., Krystofinski, P.,
 424 Li, H., *et al.* (2018). Reprogramming human T cell function and specificity with non-viral genome
 425 targeting. *Nature* 559, 405-409.

426 Schmid, M., Durussel, T., and Laemmli, U.K. (2004). ChIC and ChEC; genomic mapping of
 427 chromatin proteins. *Mol Cell* 16, 147-157.

428 Schubert, C. (2018). Technology Feature: ChIP off the old block: Beyond chromatin
 429 immunoprecipitation. *Science* 362, 1190-1192.

430 Skene, P.J., Henikoff, J.G., and Henikoff, S. (2018). Targeted in situ genome-wide profiling with
 431 high efficiency for low cell numbers. *Nat Protoc* 13, 1006-1019.

432 Skene, P.J., and Henikoff, S. (2015). A simple method for generating high-resolution maps of
 433 genome wide protein binding. *eLife* 4, e09225.

434 Skene, P.J., and Henikoff, S. (2017). An efficient targeted nuclease strategy for high-resolution
 435 mapping of DNA binding sites. *eLife* 6, e21856.

436 Teves, S.S., An, L., Hansen, A.S., Xie, L., Darzacq, X., and Tjian, R. (2016). A dynamic mode of
 437 mitotic bookmarking by transcription factors. *eLife* 5, e22280.

438 Teytelman, L., Thurtle, D.M., Rine, J., and van Oudenaarden, A. (2013). Highly expressed loci are
 439 vulnerable to misleading ChIP localization of multiple unrelated proteins. *Proc Natl Acad Sci U S*
 440 *A* 110, 18602-18607.

441 Thakur, J., and Henikoff, S. (2018). Unexpected conformational variations of the human
 442 centromeric chromatin complex. *Genes Dev* 32, 20-25.

443 Uyehara, C.M., and McKay, D.J. (2019). A direct and widespread role for the nuclear receptor
 444 EcR in mediating the response to ecdysone in *Drosophila*. *bioRxiv*
 445 <https://www.biorxiv.org/content/early/2019/01/10/517458>.

446 van Galen, P., Viny, A.D., Ram, O., Ryan, R.J., Cotton, M.J., Donohue, L., Sievers, C., Drier, Y.,
 447 Liao, B.B., Gillespie, S.M., *et al.* (2016). A Multiplexed System for Quantitative Comparisons of
 448 Chromatin Landscapes. *Mol Cell* 61, 170-180.

449 Weber, C.M., Ramachandran, S., and Henikoff, S. (2014). Nucleosomes are context-specific,
 450 H2A.Z-modulated barriers to RNA polymerase. *Mol Cell* 53, 819-830.

451 Zhang, W., Chen, Z., Yin, Q., Zhang, D., Racowsky, C., and Zhang, Y. (2019). Maternal-biased
 452 H3K27me3 correlates with paternal-specific gene expression in the human morula. *Genes Dev*
 453 33, 382-387.

454 Zheng, X.Y., and Gehring, M. (2019). Low-input chromatin profiling in *Arabidopsis* endosperm
 455 using CUT&RUN. *Plant reproduction* 32, 63-75.

456

457

H3K27me3	Ab first	BSA	Human	Yeast	E. coli	Corr (Sc:Ec)
pA lo-hi			5913983	743	3455	0.92
pA lo-hi		+	7748003	858	4988	
pA lo-hi	+		5202278	2288	16110	
pA lo-hi	+	+	5178086	1804	18759	
pA std			6013347	595	2462	0.99
pA std		+	6005080	859	2295	
pA std	+		4104736	2624	21236	
pA std	+	+	3972820	2328	19245	
pAG lo-hi			6999802	789	404	0.94
pAG lo-hi		+	6374939	642	467	
pAG lo-hi	+		4140407	1565	1291	
pAG lo-hi	+	+	4058693	2382	5289	
pAG std			7514127	308	567	0.90
pAG std		+	5935592	355	125	
pAG std	+		4594153	1271	555	
pAG std	+	+	5379610	2509	1353	

Table 1. Carry-over *E. coli* DNA correlates closely with the heterologous spike-in for both fusion proteins and both low-salt/high-calcium and standard digestion conditions. CUT&RUN was performed for H3K27me3 in parallel for pA/MNase Batch #6 (pA), pAG/MNase (pAG) using both low-salt/high-calcium (lo-hi) and standard (std) CUT&RUN digestion conditions. Each sample started with ~700,000 cells and 10 μ L of bead slurry. Also varied in this experiment was addition of antibody followed by bead addition (Ab first) and addition of 0.1% BSA in the antibody buffer (BSA). Adding antibody first led to increased recovery of both yeast and *E. coli* DNA relative to human DNA, indicative of loss of cells prior to addition of fusion protein, possibly caused by loss of digitonin solubilization of membrane sugars.

Figure Legends

Figure 1. An improved fusion protein for CUT&RUN. A) Schematic diagram (not to scale) showing improvements to the pA-MNase fusion protein, which include addition of the C2 Protein G IgG binding domain, a 6-histidine tag for purification and a hemagglutinin tag (HA) for immunoprecipitation. **B)** The Protein A/G hybrid fusion results in high-efficiency CUT&RUN for both rabbit and mouse primary antibodies. CUT&RUN for both rabbit and mouse RNAPII-Ser5phosphate using pAG/MNase were extracted from either the supernatant or the total cellular extract. Tracks are shown for the histone gene cluster at Chr6:26,000,000-26,300,000, where NPAT is a transcription factor that co-activates histone genes. Tracks for 2' and 10' time points are displayed at the same scale for each antibody and for both supernatant (supn) or total DNA extraction protocols.

Figure 2. Targeted fragments are not released during digestion using high-calcium/low-salt conditions. CUT&RUN was performed using either the high- Ca^{++} /low-salt (Ca^{++}) or the standard (Std) method with antibodies to three different epitopes. DNA was extracted from supernatants, where no elution was carried out for the Ca^{++} samples. Although high yields of nucleosomal ladder DNA eluted from the supernatants using the standard method, no DNA was detectable in the supernatant using the high- Ca^{++} /low salt method when the elution step was omitted. Left, Tapestation images from indicated lanes; Right, Densitometry of the same lanes.

Figure 3. Similar performance using pA/MNase and pAG/MNase. A) CUT&RUN was performed with an antibody to H3K27ac (Millipore MABE647) and to CTCF (Millipore 07-729) with digestion over a 1 to 27 min range as indicated using pAG/MNase with the high- Ca^{++} /low-salt protocol. Correlation matrix comparing peak overlap for time points and fusion constructs. The datasets were pooled and MACS2 was used with default parameters to call peaks, excluding those in repeat-masked intervals and those where peaks overlapped with the top 1% of IgG occupancies, for a total of 52,425 peaks. Peak positions were scored for each dataset and correlations (R^2 values shown along the diagonal and displayed with Java TreeView v.1.16r2, contrast = 1.25) were calculated between peak vectors. IgG and H3K27me3 (me3) negative controls were similarly scored. **B)** Same as A, except the antibody was to CTCF. A set of 9,403 sites with a CTCF motif within a hypersensitive site was used (Skene & Henikoff, 2017). High correlations between all time points demonstrate the uniformity of digestion over a 27-fold range. **C)** Representative tracks from datasets used for panels A and B showing a 100-kb region that includes a histone locus cluster (chr6:25,972,600-26,072,600).

Figure 4. Consistent peak definition with high- Ca^{++} /low salt digestion. A) H3K27ac CUT&RUN time-course experiments were performed with an Abcam 4729 rabbit polyclonal antibody, following either the standard protocol or the low-salt/high-calcium (High- Ca^{++}) protocol. Samples of 5 million fragments from the 10 H3K27ac datasets were pooled and MACS2 called 36,529 peaks. Peak positions were scored for each dataset and correlations (R^2 values shown along the diagonal) were calculated between peak vectors. IgG and H3K27me3 (me3) negative controls were similarly scored. Higher correlations between the High- Ca^{++} than the Standard time points indicates improved uniformity of digestion over the ~100-fold range of digestion

times. **B)** Tracks from a representative 200 kb region around the HoxB locus. **C)** Fraction of reads in peaks (Frip) plots for each time point after down-sampling (5 million, 2.5 million, 1.25 million, 625,000 and 312,500), showing consistently higher Frip values for Ca⁺⁺ (red) than Std (blue).

Figure 5. *E. coli* carry-over DNA of pA/MNase and pAG/MNase can substitute for spike-in

calibration. A) Fragments from a CUT&RUN K562 cell experiment (GSE104550 20170426) using antibodies against H3K27me3 (100-8,000 cells) and CTCF (1,000-100,000 cells) were mapped to the repeat-masked genome of *S. cerevisiae* and the full genome *E. coli*. Standard digestion was followed by supernatant release and extraction. **B)** Same as A using antibodies against multiple epitopes of varying abundances, with high-calcium/low-salt digestion followed by supernatant release and extraction. **C)** Same as B except using standard digestion conditions and total DNA extraction. The *S. cerevisiae* spike-in DNA was left out for one sample (blue square). From top to bottom, antibodies are: NPAT Thermo PA5-66839, Myc: CST Rabbit Mab #13987, CTD: PolII CTD Abcam 8WG16, RNAPII-Ser5: Abcam 5408 (mouse), RNAPII-Ser2: CST E1Z3G, CTCF Millipore 07-729, RNAPII-Ser5: CST D9N5I (rabbit), H3K4me2: Upstate 07-030. **D)** Same as C except using high-calcium/low-salt digestion and total DNA extraction. From top to bottom, antibodies are: CTCF Millipore 07-729, NPAT Thermo PA5-66839, Myc: CST Rabbit Mab #13987, CTD: PolII CTD Abcam 8WG16, RNAPII-Ser5: Abcam 5408 (mouse), RNAPII-Ser5: CST D9N5I (rabbit), RNAPII-Ser2: CST E1Z3G, H3K4me2: Upstate 07-030.

Supplementary Figure Legends

Figure 1 – figure supplement 1. An improved fusion protein for CUT&RUN. A) Plasmid map of pAG-ERH-MNase-6xHIS-HA. **B)** Coomassie-stained gel of fusion protein eluted from nickel-agarose.

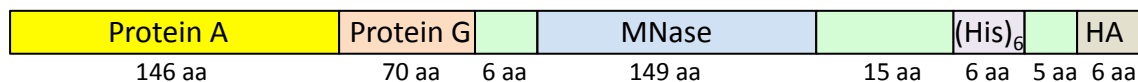
Figure 1 – figure supplement 2. pAG/MNase titration. A) K562 cells were incubated with an antibody to H3K27me3 (CST #9733 Rabbit monoclonal), washed twice with 1 ml Dig-wash. The sample was split into aliquots for incubation with pA/MNase at the recommended concentration and a serial dilution of pAG/MNase, followed by 3 1 ml washes. After 30 min using the standard protocol, limit digestions are seen at all dilutions for this abundant epitope, indicating that the amount of fusion protein used in this experiment was in excess. **B)** Representative tracks from these samples on the same normalized count scale show consistently low CUT&RUN backgrounds with excess pAG/MNase, which indicates that washes are sufficient to minimize non-specific background cleavages. ENCODE ChIP-seq tracks are shown for comparison, where USC used CST #9733, and Broad Institute used Millipore 07-449.

Figure 4 – figure supplement 1. CUT&RUN consistency with high-Ca⁺⁺/low salt digestion and total DNA extraction. A) H3K4me2 CUT&RUN time points with digestions using either the standard protocol or the high-calcium/low-salt protocol with either supernatant or total DNA extraction. To construct the correlation matrix, all 8 H3K4me2 datasets were pooled and MACS2 was used to call peaks, which yielded 64,156 peaks. Peak positions were scored for each dataset and correlations (R^2 displayed with Java TreeView v.1.16r2, contrast = 1.25) were calculated between peak vectors. IgG and H3K27me3 (me3) negative controls were similarly scored. **B)** Same as Figure 4B. **C)** Same as Figure 4C.

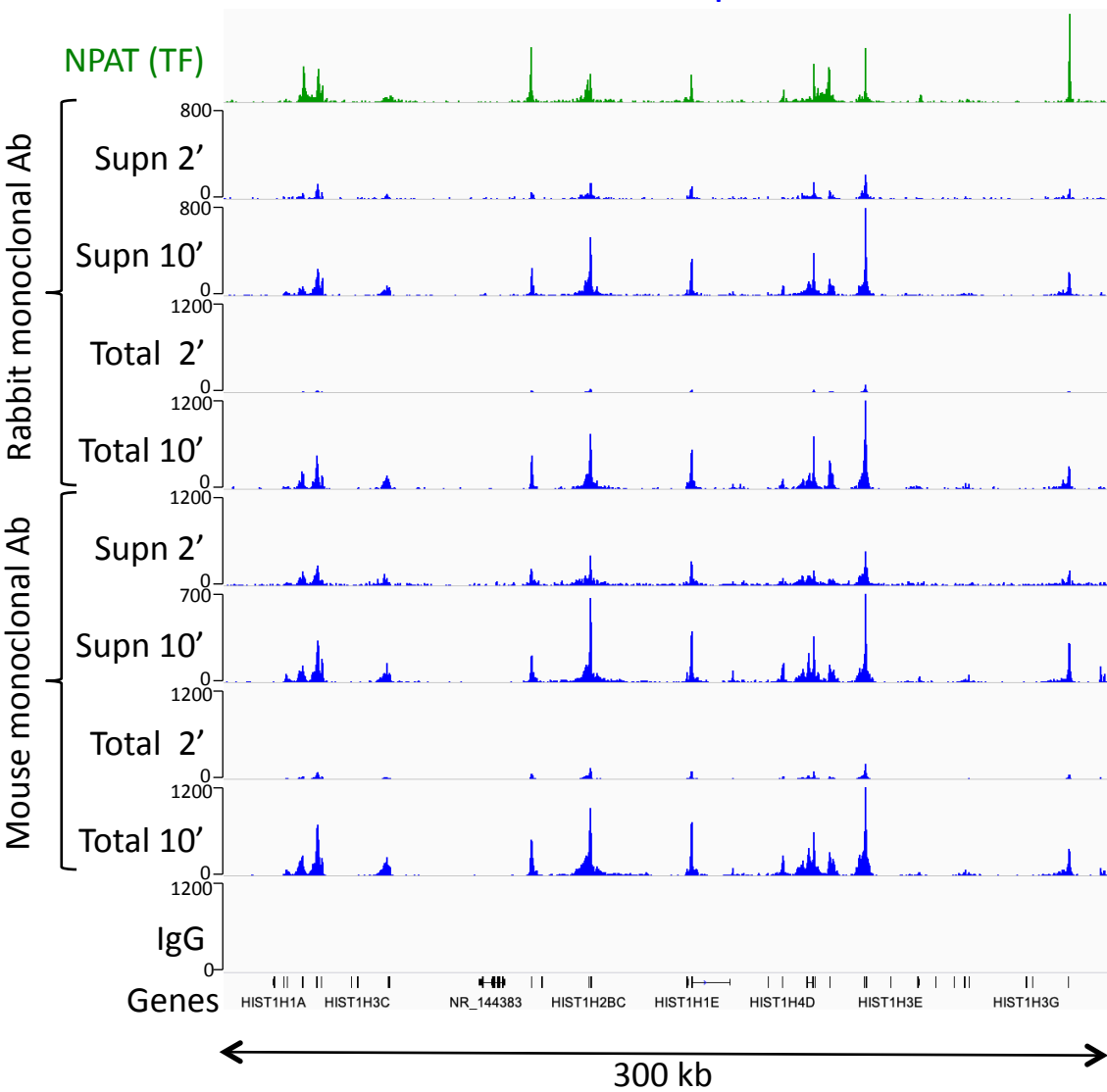
Figure 4 – figure supplement 2. Tapestation analyses of an H3K27ac digestion time-course series. CUT&RUN with the low-salt/high-calcium protocol results in fragment release within 20 seconds at 0 °C.

A

pAG-ERH-MNase-6xHIS-HA (pAG/MNase) expression cassette (45 kDa)

**B**

RNA PolII-Ser5phos



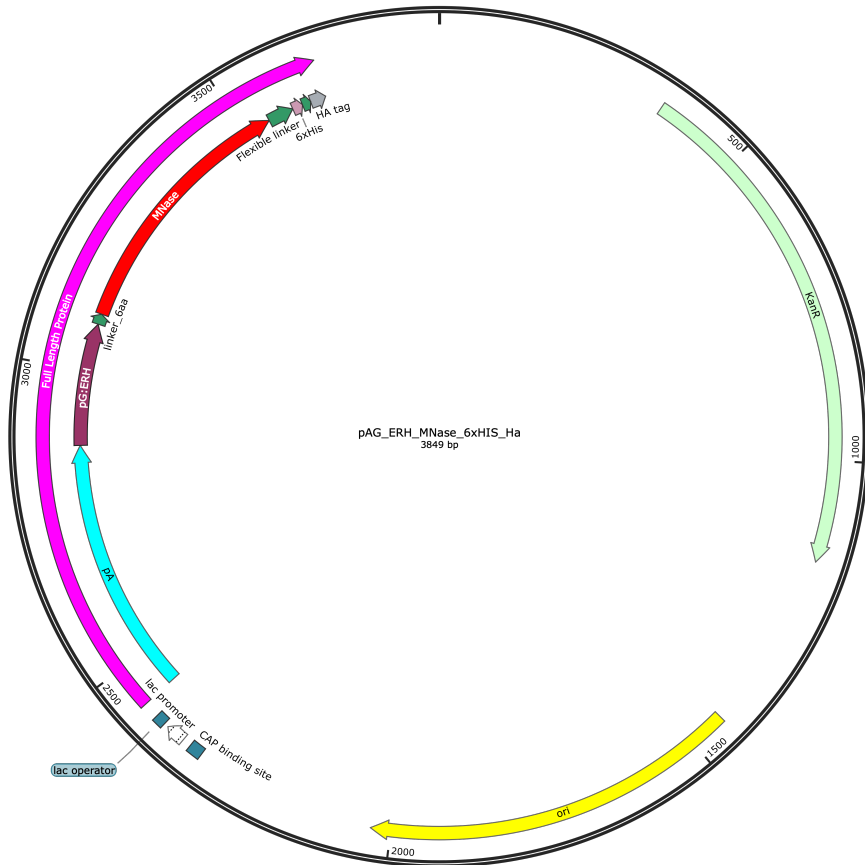
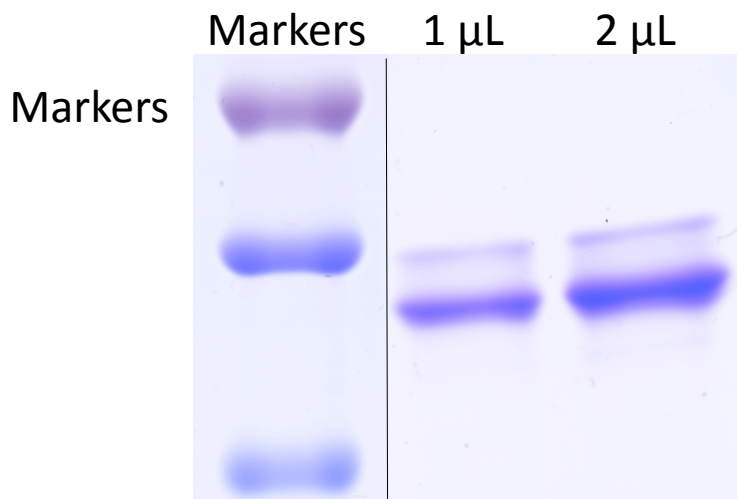
A**B**

Figure 1 – figure supplement 1. An improved fusion protein for CUT&RUN. A) Plasmid map of pAG-ERH-MNase-6xHIS-HA. **B)** Coomassie-stained gel of fusion protein eluted from nickel-agarose.

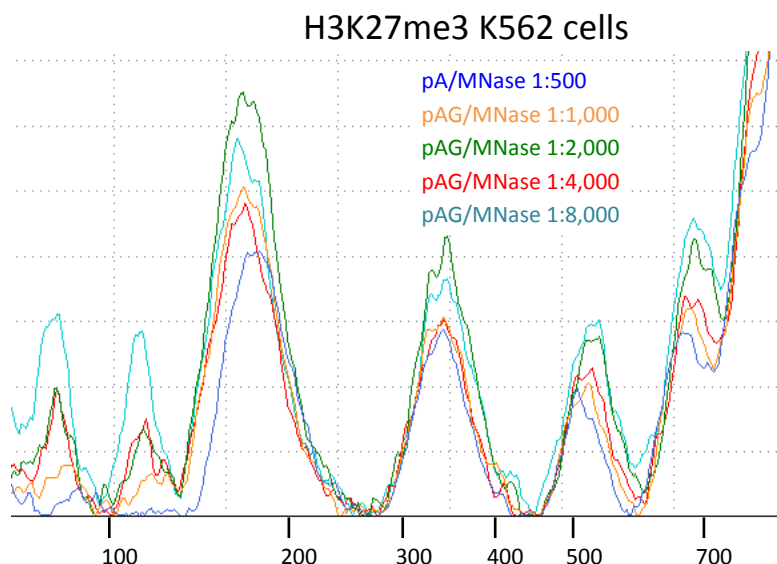
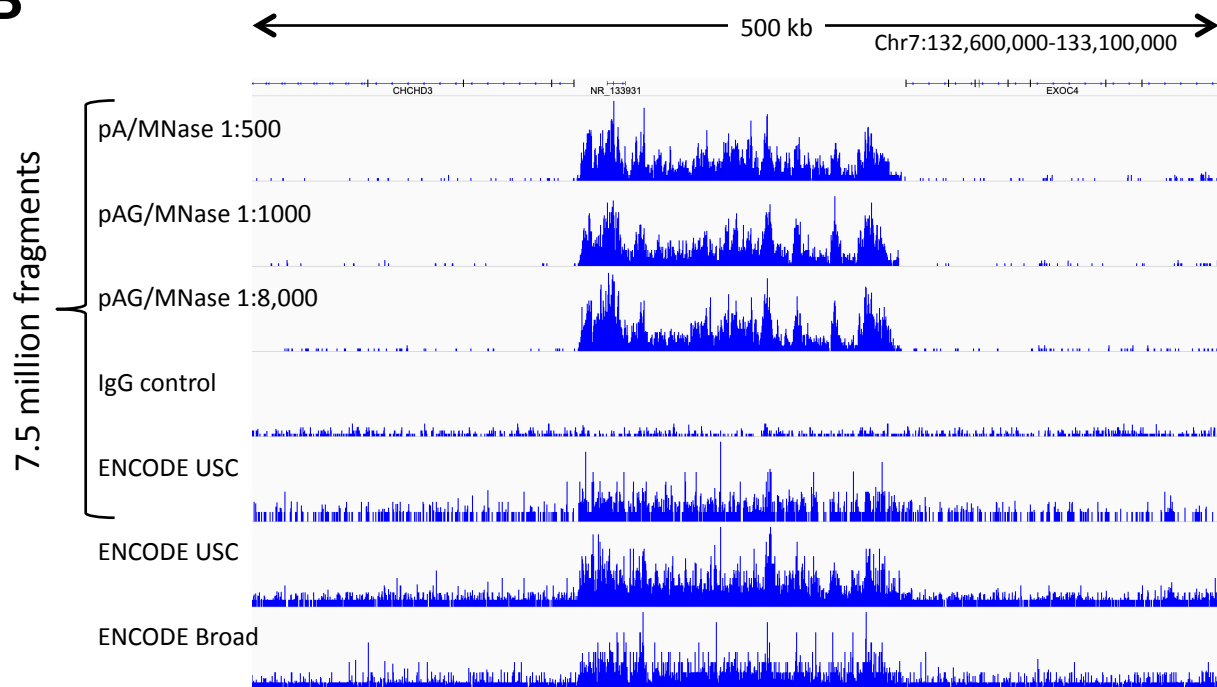
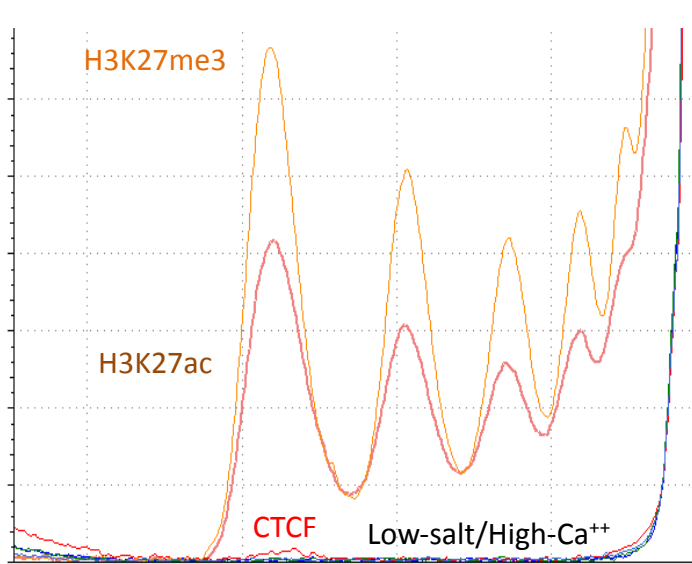
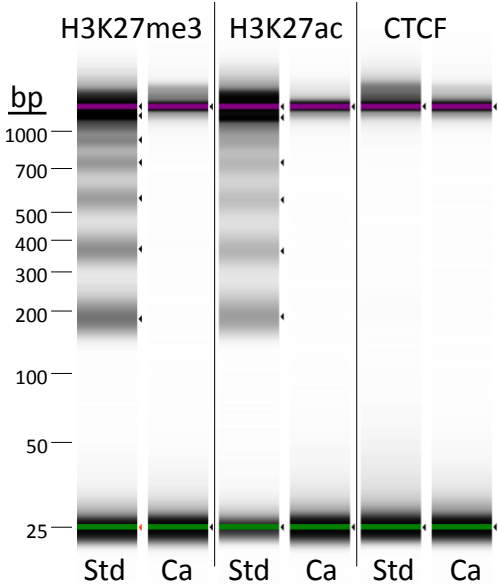
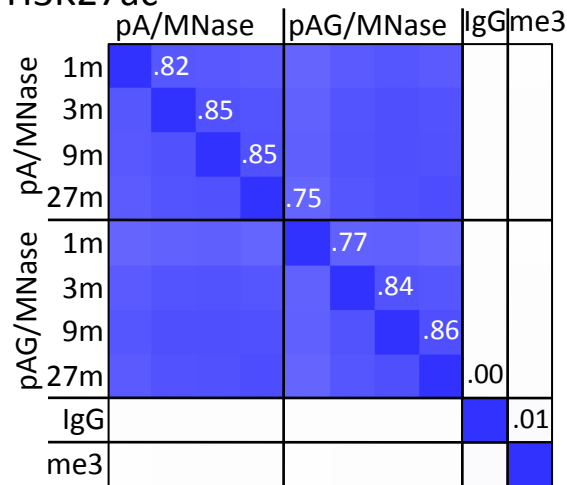
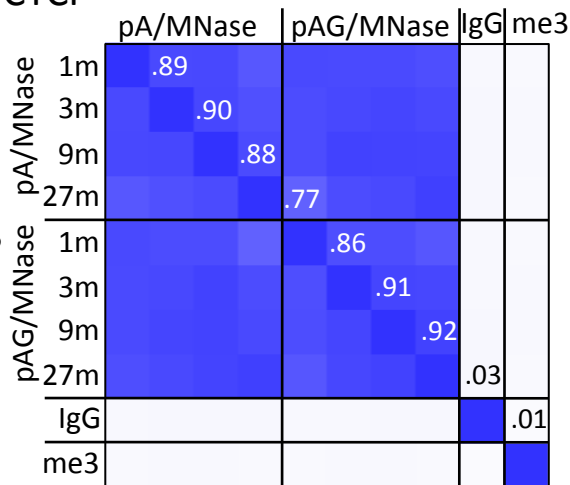
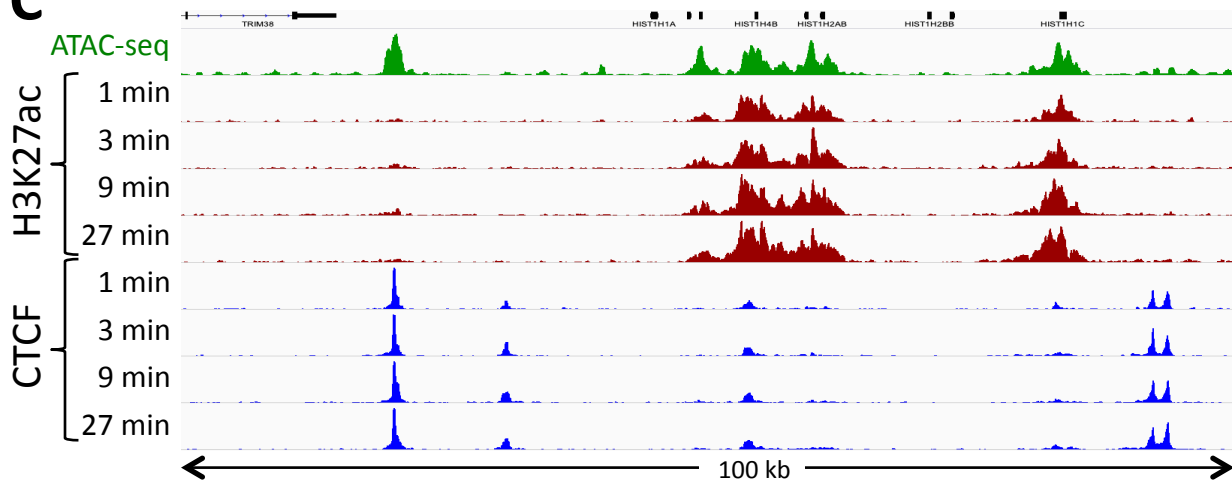
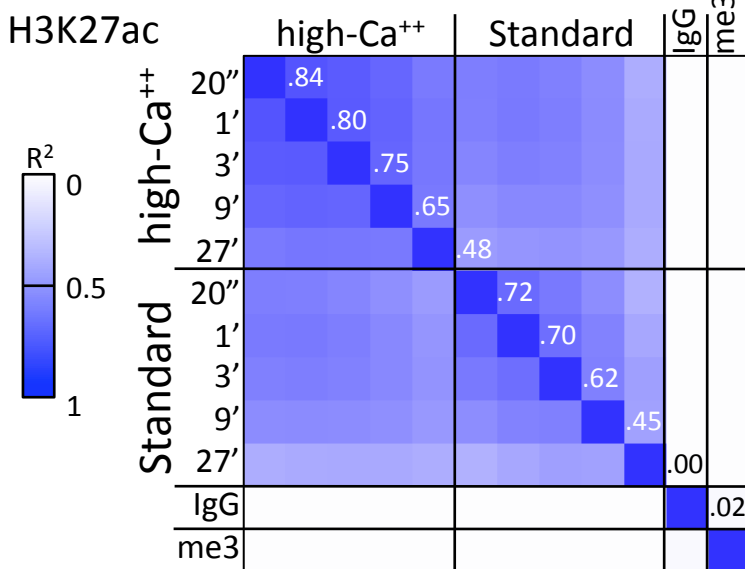
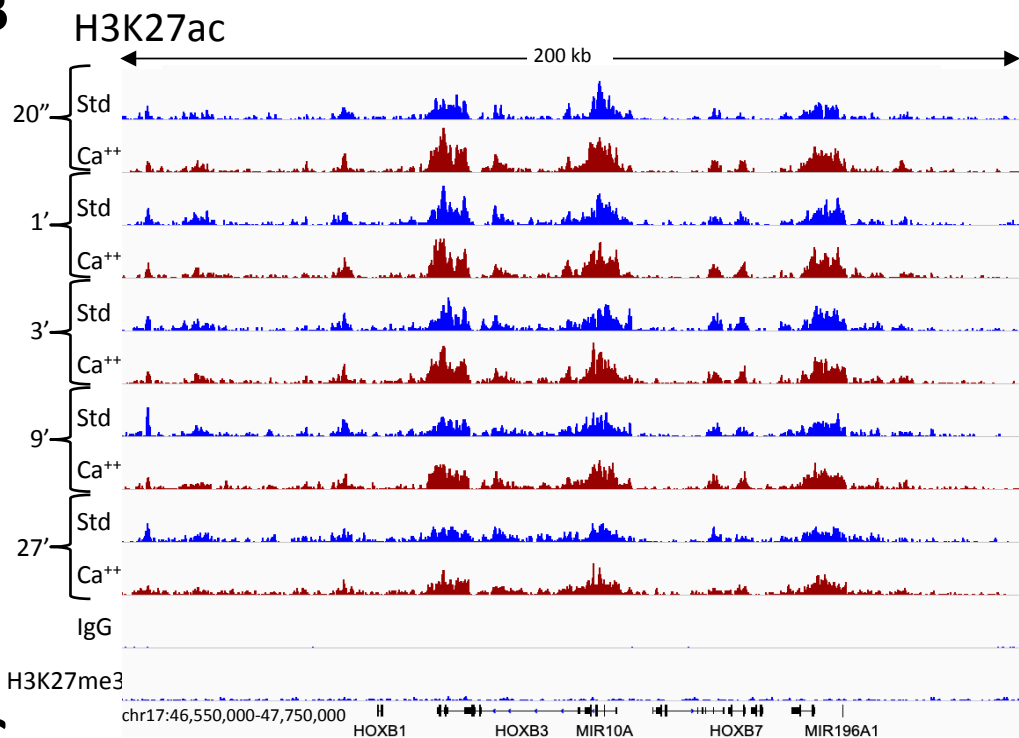
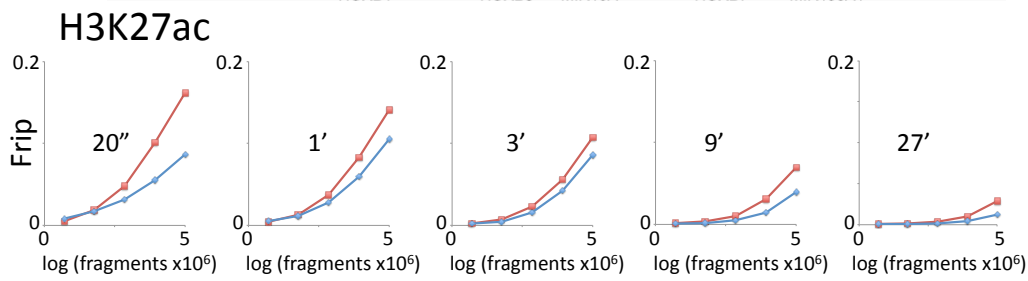
A**B**

Figure 1 – figure supplement 2. pAG/MNase titration. A) K562 cells were incubated with an antibody to H3K27me3 (CST #9733 Rabbit monoclonal), washed twice with 1 ml Dig-wash. The sample was split into aliquots for incubation with pA/MNase at the recommended concentration and a serial dilution of pAG/MNase, followed by 3 1 ml washes. After 30 min using the standard protocol, Ilmit digestions are seen at all dilutions for this abundant epitope, indicating that the amount of fusion protein used in this experiment was in excess. **B)** Representative tracks from these samples on the same normalized count scale show consistently low CUT&RUN backgrounds with excess pAG/MNase, which indicates that washes are sufficient to minimize non-specific background cleavages. ENCODE ChIP-seq tracks are shown for comparison, where USC used CST #9733, and Broad Institute used Millipore 07-449.



A**H3K27ac****B****CTCF****C**

A**B****C**

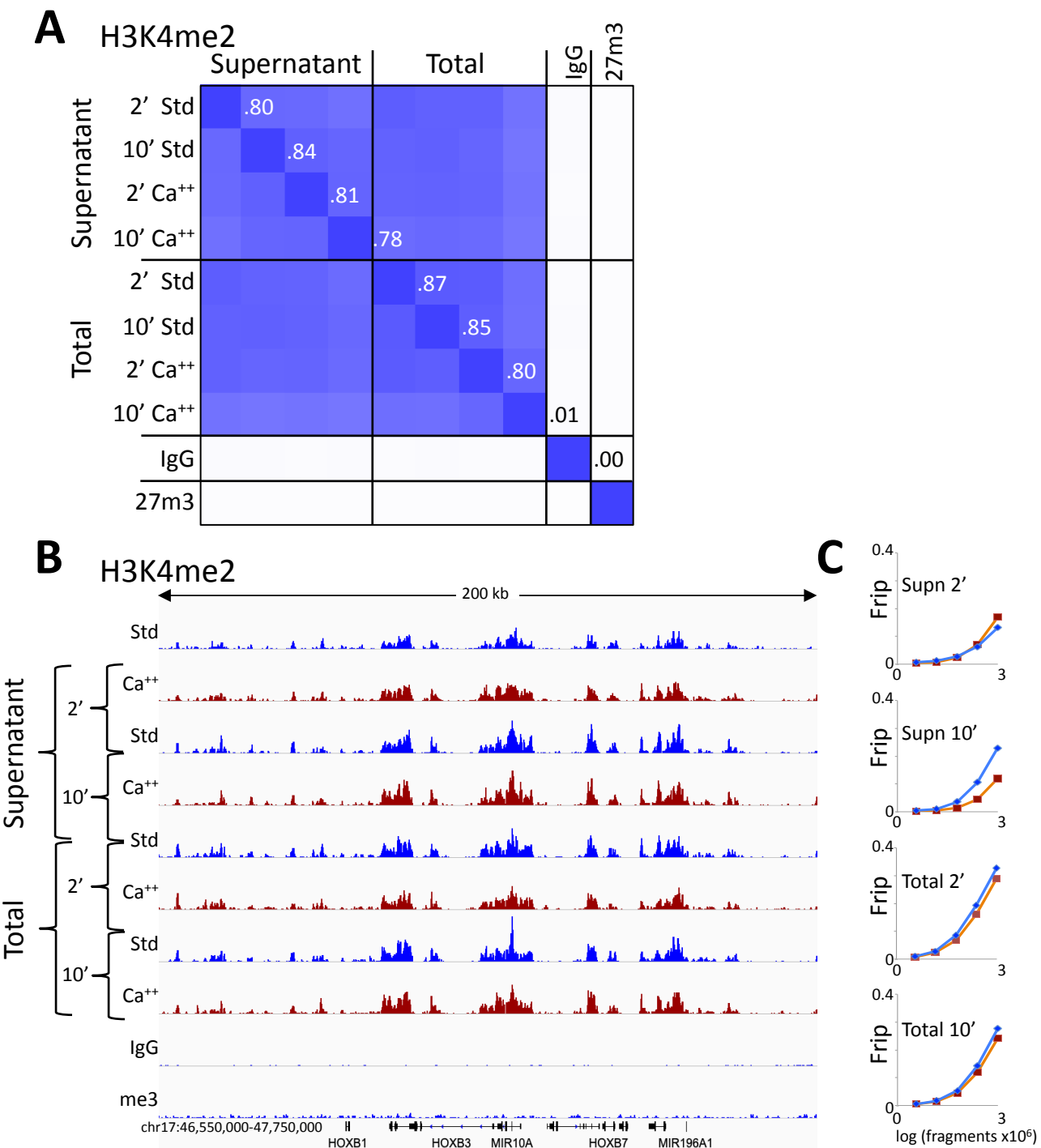
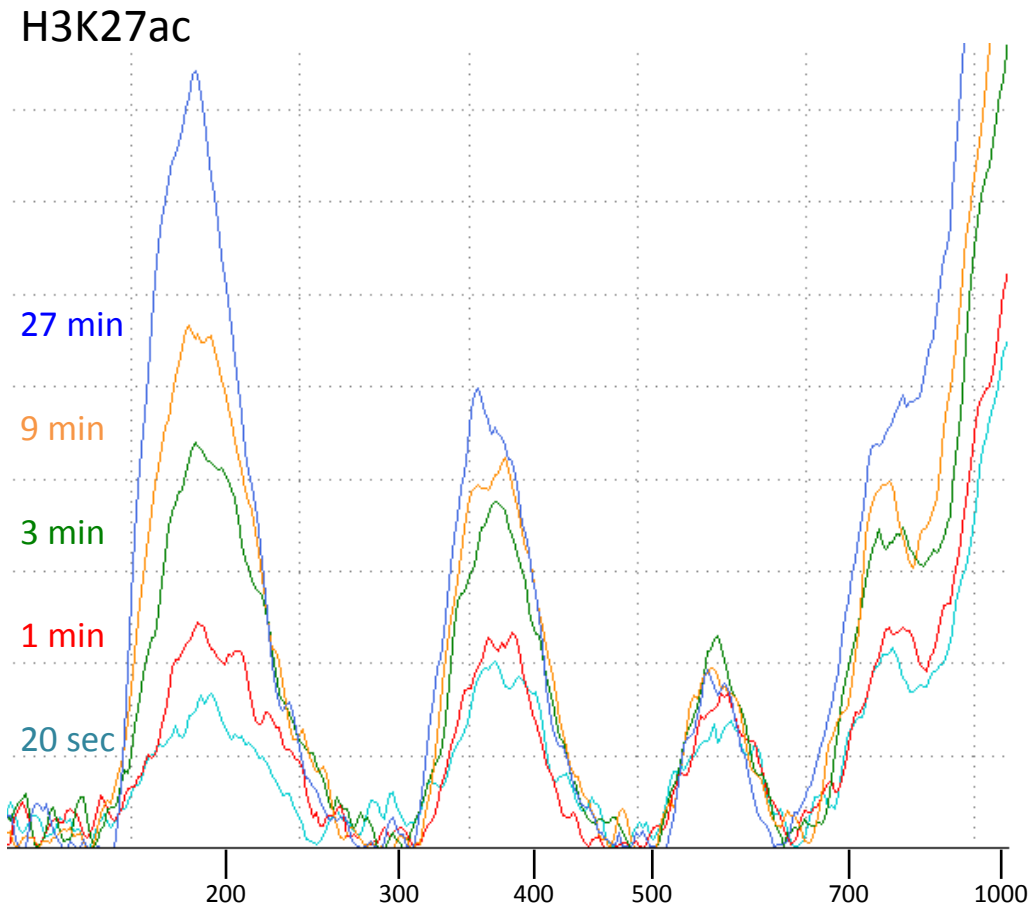
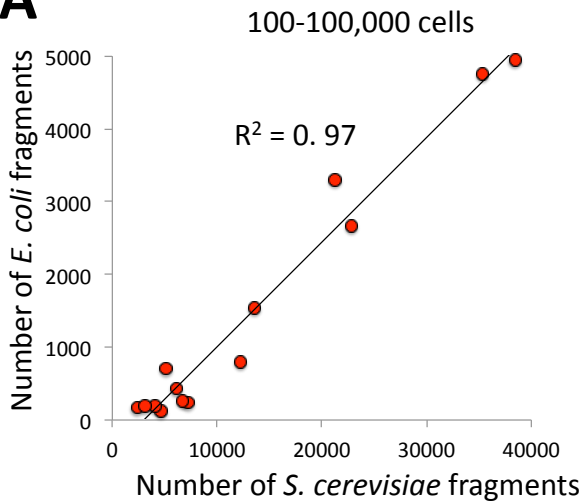
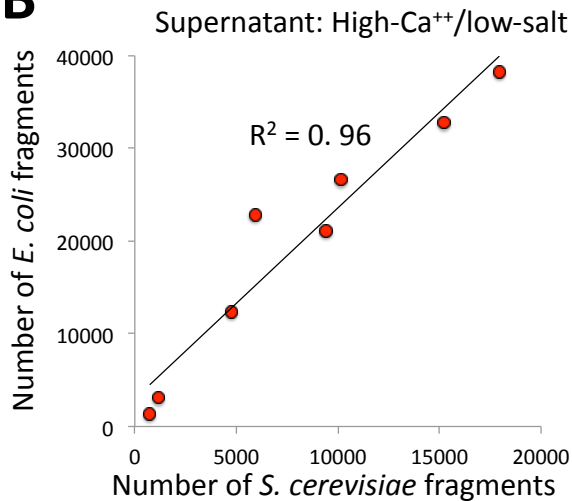
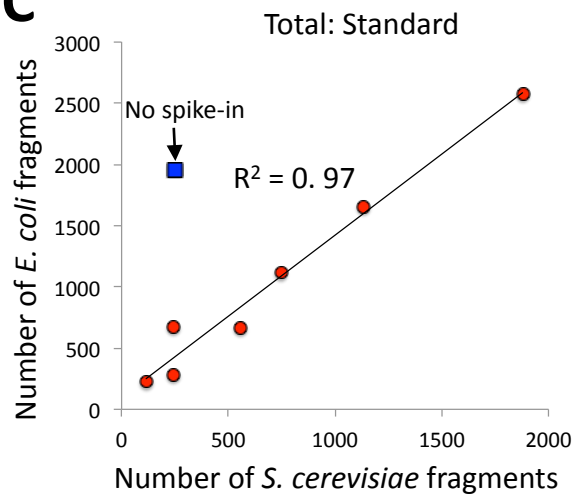


Figure 4 – figure supplement 1. CUT&RUN consistency with high-Ca⁺⁺/low salt digestion and total DNA extraction. **A)** H3K4me2 CUT&RUN time points with digestions using either the standard protocol or the high-calcium/low-salt protocol with either supernatant or total DNA extraction. To construct the correlation matrix, all 8 H3K4me2 datasets were pooled and MACS2 was used to call peaks, which yielded 64,156 peaks. Peak positions were scored for each dataset and correlations (R^2 displayed with Java TreeView v.1.16r2, contrast = 1.25) were calculated between peak vectors. IgG and H3K27me3 (me3) negative controls were similarly scored. **B)** Same as Figure 4B. **C)** Same as Figure 4C.

H3K27ac

27 min
9 min
3 min
1 min
20 sec



A**B****C****D**